Diagnostic performance of the beam emission spectroscopy system on the National Spherical Torus Experiment[a)]

D. R. Smith,[b)] R. J. Fonck, G. R. McKee, and D. S. Thompson
Department of Engineering Physics, University of Wisconsin-Madison, Madison, Wisconsin 53706, USA

(Presented 8 May 2012; received 8 May 2012; accepted 21 May 2012; published online 11 June 2012)

The beam emission spectroscopy system on the National Spherical Torus Experiment measures localized density fluctuations on the ion gyroscale. Optical sightlines provide core to edge radial coverage, and the sightlines are aligned to typical pitch angles to maximize cross-field spatial resolution. Sightline images are 2–3 cm, and point spread function calculations indicate image distortion from pitch angle misalignment and atomic state finite lifetimes is minor with a 15% increase in the image size. New generation photodetectors achieve photon noise limited measurements at frequencies up to 400 kHz with refrigerant cooling at −20 °C. Measurements near the pedestal show broadband turbulence up to 100 kHz, and poloidal correlation lengths are about 10 cm. Plasma turbulence signals can be 2–3 orders of magnitude above photon noise and amplifier thermal noise. © *2012 American Institute of Physics*. [http://dx.doi.org/10.1063/1.4728094]

The beam emission spectroscopy (BES) diagnostic system on NSTX (Ref. 1) measures D_α emission ($n = 3 \rightarrow 2$, $\lambda_0 = 656.1$ nm) from deuterium heating beams.[2] BES measurements are sensitive to ion gyroscale fluctuations associated with low wavenumber (low-k) turbulence and Alfvén modes. The beam velocity induces a Doppler shift in beam emission, and optical filters isolate beam D_α emission from thermal D_α emission. The intersection of optical sightlines with the neutral beam volume provides spatial localization, but a rigorous assessment of spatial and k-space measurement properties require point spread function calculations.[3] BES measurements are sensitive to plasma density fluctuations according to $\delta I_{D\alpha}/I_{D\alpha} = C\,(\delta n/n)$ where $C = C(E_{NB}, n, T_e, Z_{eff}) \approx 1/2$.[2]

The NSTX BES system includes two optical assemblies centered at $r/a \approx 0.45$ and 0.85.[1] The optical views are pitched upward at 26° and 37° for alignment with typical NSTX pitch angles to optimize cross-field spatial resolution. As shown in Figure 1, 56 sightlines provide core-to-SOL radial coverage and four discrete poloidal arrays, and sightline images are 2–3 cm at the neutral beam. The measurements are sensitive to fluctuations with $k_\perp \rho_s \lesssim 1.5$ where $\rho_s \approx 0.5$–1.5 cm ($\rho_s \equiv \sqrt{2 m_i T_e}/qB$ is the ion sound gyroradius). High throughput optics collect light at f/1.5 with 2.3 mm^2-ster étendue and image the light onto 9-fiber optical bundles for transmission to photodetectors. Interference filters with 4 nm passbands at 661 nm pass redshifted D_α emission from deuterium heating beams and block thermal D_α emission. At normal incidence, the interference filters pass full energy and 1/2 energy beam components, but 1/3 energy components near Carbon-II lines are attenuated. Tuning the filters to lower wavelength can pass 1/3 energy components and Carbon-II emission. Note that emission spectra from motional Stark effect and fast ion D_α diagnostics indicate the C-II emission is comparable to or less than the neutral beam D_α manifold.[1] New generation PIN photodiode detectors and frequency-compensating, wideband preamplifiers provide photon-noise limited measurements at frequencies up to 400 kHz with refrigerant (non-cyrogenic) cooling at −20 °C.[1,4] The data acquisition system samples at 2 MHz (output) with an onboard field programmable gate array (FPGA) post-processor circuit. The FPGA functions as a finite impulse response filter to suppress high frequency thermal noise. The wideband, low noise detectors enable measurements of high frequency Alfvén and energetic particle modes up to about 800 kHz in addition to low-k turbulence at low frequency.

The BES poloidal array at $R = 140$ cm provides multipoint measurements for calculating the spatial and temporal properties of turbulence. Figure 2 shows example BES measurements at two radial locations. Note that BES signals change sharply at NBI steps, and BES auto-power spectra can exceed photodetector dark noise power spectra by 2–3 orders of magnitude. Poloidally separated channels in the $R = 140$ cm poloidal array ($r/a \approx 0.80$–0.95) (see Figure 1) provide measurements of the poloidal correlation length L_c, decorrelation time τ_d, and poloidal wavenumber k_θ associated with low-k turbulence. Coherence spectra in Figure 3 show reduced coherence with greater poloidal separation, as expected, and cross-phase spectra show greater cross-phase with greater poloidal separation. Autopower spectra (Figure 3(c)) show plasma turbulence signals 2–3 orders of magnitude greater than dark noise and photon noise levels, and filtered data (Figure 3(d)) show turbulent eddies propagating along the poloidal array. The turbulence quantities are derived from time-lag auto- and cross-correlation functions in Figure 3(e). Data windows of 15–40 ms are segmented into 30–150 bins with 512–2048 time points per bin. The time-lag correlation functions for each bin are averaged to obtain the average time-lag correlation function and variance for the data window. The cross-correlation envelope (Hilbert transform) at zero

[a)]Contributed paper, published as part of the Proceedings of the 19th Topical Conference on High-Temperature Plasma Diagnostics, Monterey, California, May 2012.

[b)]Electronic mail: drsmith@engr.wisc.edu.

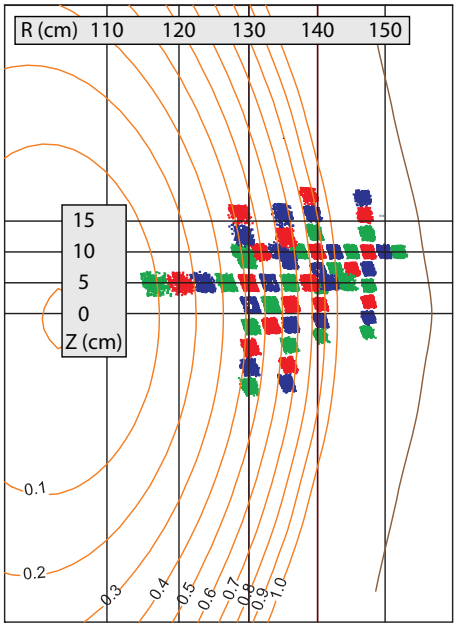

FIG. 1. BES sightlines provide radial coverage from core to scrape-off-layer regions and four discrete poloidal arrays.

time-lag decreases with channel separation, and the poloidal correlation length L_c is the corresponding $1/e$ length as shown in Figure 3. The time-lag of the peak cross-correlation envelope increases with channel separation, and the linear relationship gives the eddy velocity v_g. The peak cross-correlation envelope decreases with time-lag, and the decorrelation time τ_d is the corresponding $1/e$ time-lag. The poloidal wavenumber k_θ is derived from the eddy size inferred from the eddy velocity and the time-lab between auto-correlation anti-nodes. Finally, note that coherence spectra are above statistical uncertainties at frequencies below about 35 kHz in Figure 3(a),

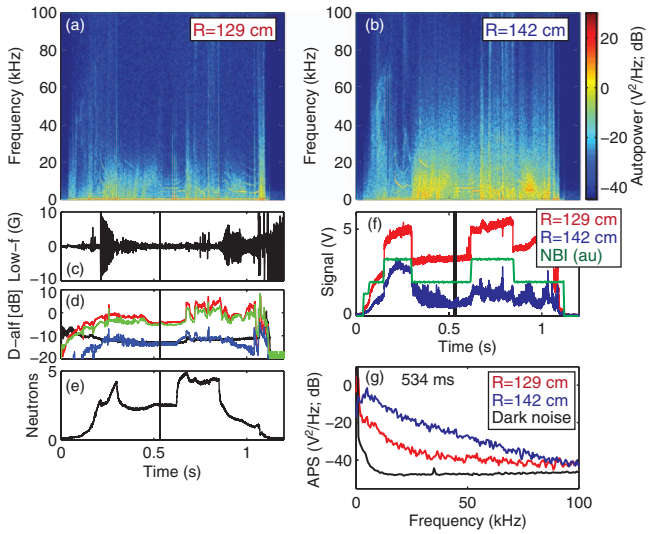

FIG. 2. BES auto-power spectrograms for measurements at (a) $R = 129$ cm and (b) 142 cm; (c) low frequency odd-n magnetic fluctuations; (d) thermal D_α emission measurements; (e) neutron measurements; (f) BES time-series data with NBI power (green line); and (g) BES auto-power spectra at 534 ms with photodetector dark noise spectrum.

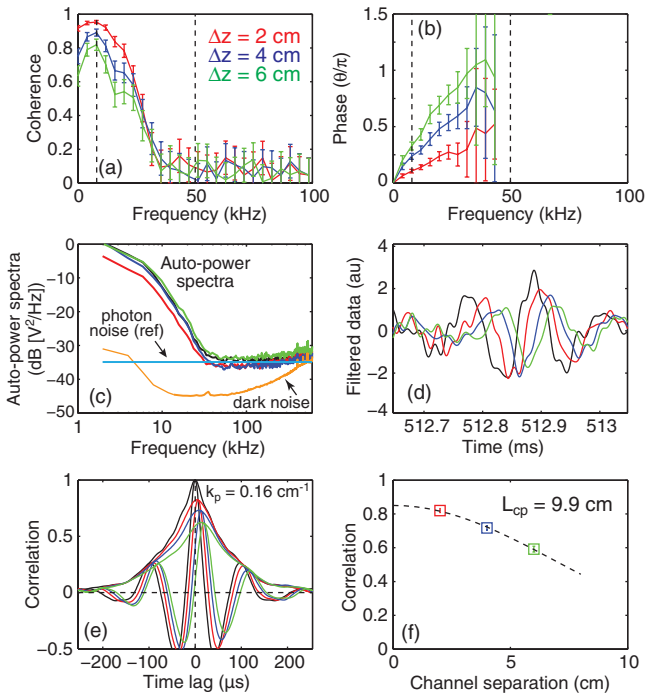

FIG. 3. (a) Coherence and (b) cross-phase spectra among four channels in the BES $R = 140$ cm poloidal array during an ELM-free, MHD quiescent period; (c) auto-power spectra and photon and dark noise for reference channel; (d) filtered data (8–50 kHz) used for calculations in (e) and (f); (e) time lag auto- and cross-correlation functions and envelopes; and (f) correlation envelope at zero time lag vs. channel separation. Black line in (c)–(e) denotes reference channel.

consistent with autopower spectra exceeding noise levels at frequencies below about 35 kHz in Figure 3(c).

Backlight fiber images are 2–3 cm at the center of the neutral beam, but accurate spatial and k-space characterization of BES measurements require point spread function (PSF) calculations.[3] PSF calculations convolve optical system properties with neutral beam profiles, plasma geometry, and atomic state lifetimes[5] that distort the optical image. For tokamak geometry, PSF calculations can ignore small pitch angle corrections and reduce the calculation to 2D without compromising accuracy, but steep ST pitch angles require full 3D PSF calculations. Figure 4 shows fiber bundle images at $R = 133$, 140, and 143 cm. At $R = 140$ and 143 cm, excited state lifetimes in the low density edge region dominate image distortion. At $R = 133$ cm, magnetic field misalignment dominates image distortion. Without excited state lifetime and magnetic field geometry effects, fiber images are 3.75 cm across at full-width half-max (FWHM, 50% of peak intensity). With the effects, the FWHM images are in the range 3.6–3.9 cm, so image distortion from atomic excited states and field line geometry is mild.

In summary, the BES diagnostic system on NSTX measures density fluctuations on the ion gyroscale to investigate low-k turbulence and Alfvén modes. Sightline images are 2–3 cm at the neutral beam, and point spread function calculations indicate image distortion from field line misalignment and atomic state lifetimes are minor.

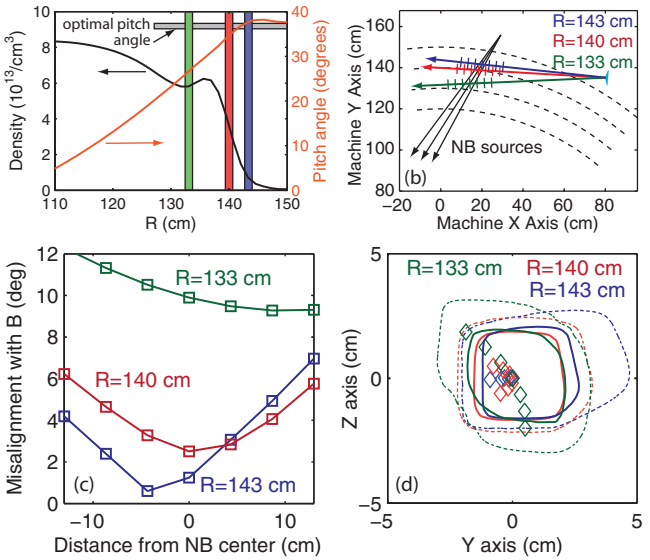

FIG. 4. (a) NSTX density and pitch angle profiles with BES measurements at $R = 133$, 140, and 143 cm; (b) BES sightlines crossing neutral beam sources, and short cross-lines show imaging planes; (c) sightline misalignment with magnetic field along sightlines; and (d) PSF image contours at 50% (solid) and 10% (dashed) of peak intensity with magnetic field puncture points (diamonds) on successive image planes.

New generation photodetectors with refrigerant cooling at −20 °C achieve photon noise limited measurements at frequencies up to 400 kHz with plasma turbulence signals 2–3 orders of magnitude above noise signals. Initial measurements show broadband turbulence near the pedestal top with frequencies up to 100 kHz and poloidal correlation lengths around 10 cm. Two-megahertz sampling and anti-alias filters enable Alfvèn mode measurements at frequencies up to 800 kHz.

This work was supported by (U.S.) Department of Energy (DOE) Grant Nos. DE-FG02-89ER53296, DE-SC0001288, and DE-AC02-09CH11466.

[1]D. R. Smith, H. Feder, R. Feder, R. J. Fonck, G. Labik, G. R. McKee, N. Schoenbeck, B. C. Stratton, I. Uzun-Kaymak, and G. Winz, Rev. Sci. Instrum. **81**, 10D717 (2010).
[2]R. J. Fonck, P. A. Duperrex, and S. F. Paul, Rev. Sci. Instrum. **61**, 3487 (1990).
[3]M. W. Shafer, R. J. Fonck, G. R. McKee, and D. J. Schlossberg, Rev. Sci. Instrum. **77**, 10F110 (2006).
[4]N. Schoenbeck, S. D. Ellington, R. J. Fonck, K. Jaehnig, G. R. McKee, D. R. Smith, I. Uzun-Kaymak, and G. Winz, Rev. Sci. Instrum. **81**, 10D718 (2010).
[5]I. H. Hutchinson, Plasma Phys. Controlled Fusion **44**, 71 (2002).